applied sciences

MDPI

Article

The Exergo-Economic and Environmental Evaluation of a Hybrid Solar–Natural Gas Power System in Kirkuk

Ali Alfaris, Abdulrazzak Akroot * and Emrah Deniz

Department of Mechanical Engineering, Faculty of Engineering, Karabük University, 78050 Karabük, Turkey; ali75f@gmail.com (A.A.); edeniz@karabuk.edu.tr (E.D.)
* Correspondence: abdulrazzakakroot@karabuk.edu.tr

Abstract: The increasing environmental challenges posed by the widespread use of fossil fuels and the fluctuating nature of renewable energy have driven the need for more efficient and sustainable energy solutions. Current research is actively exploring hybrid energy systems as a means to address these issues. One such area of focus is the integration of Organic Rankine Cycles (ORCs) with gas and steam turbines, utilizing both natural gas (NG) and solar parabolic trough collectors (PTCs) as energy sources. This study examines the performance of a hybrid system implemented in Kirkuk, Iraq, a region known for its substantial solar radiation. Previous research has shown that hybrid systems can effectively enhance energy conversion efficiency and reduce environmental impacts, but there is still a need to assess the specific benefits of such systems in different geographical and operational contexts. The analysis reveals a thermal efficiency of 59.32% and an exergy efficiency of 57.28%. The exergoeconomic analysis highlights the optimal energy cost at USD 71.93/MWh when the compressor pressure ratio is set to 8 bar. The environmental assessment demonstrates a significant reduction in CO_2/emissions, with a carbon footprint of 316.3 kg CO_2/MWh at higher compressor pressure ratios. These results suggest that integrating solar energy with natural gas can substantially improve electricity generation while being both cost-effective and environmentally sustainable.

Keywords: renewable energy integration; Kirkuk power plant; exergoeconomic analysis; carbon dioxide emissions; hybrid power system

Citation: Alfaris, A.; Akroot, A.; Deniz, E. The Exergo-Economic and Environmental Evaluation of a Hybrid Solar–Natural Gas Power System in Kirkuk. *Appl. Sci.* **2024**, *14*, 10113. https://doi.org/10.3390/app142210113

Academic Editors: Sébastien Poncet and Fernando Zenaido Sierra-Espinosa

Received: 6 July 2024
Revised: 26 October 2024
Accepted: 31 October 2024
Published: 5 November 2024

1. Introduction

In today's world, energy is pivotal, serving as the foundation for economic growth and development. It is essential for industries, transportation systems, and homes; it powers and meets people's fundamental needs [1]. Climate change is heavily influenced by human activities, especially the consumption of fossil fuels in various industries. These activities result in the release of significant amounts of greenhouse gases (GHGs), specifically CO_2, CH_4, and N_2O, which contribute to the acceleration of global warming [2]. The energy domain, particularly crude oil manufacturing, serves as Iraq's economic cornerstone, driving its exports and serving as the oil refining source. It facilitates the production of various oil byproducts, including gasoline, gas oil, and liquid [3]. Electric power generation significantly contributes to global emissions, releasing various pollutants, including GHGs [4]. These emissions result from the combustion of multiple fuel types to produce electricity [5,6]. Iraq heavily depends on fossil fuels for electricity generation, a reliance that has intensified in recent years because of population growth and increasing electricity demand. The country predominantly utilizes three main fuels for electricity generation: approximately 50% of electricity production is derived from NG, 28% from fuel and crude oil, and around 15% from diesel fuel. The remaining portion accounts for electricity production from renewable sources [7]. Global concerns about fossil fuel depletion have led to renewable energy sources (RES). RES like solar energy are being explored for power generation [5,8]. Integrated solar combined cycle (ISCC) power stations are popular for

thermal power generation, but traditional direct steam generation (DSG) methods struggle with thermal efficiency [9]. PTCs have a well-established history of reliability and efficiency in large-scale solar power plants worldwide, offering a proven solution for enhancing the performance of hybrid energy systems by integrating solar thermal technology with conventional power generation [10–12]. Thermal energy-storage TES systems are being incorporated into ISCC systems to enhance efficiency, increase process flexibility, and reduce the impact of non-solar intermittency [13]. There is a consistent and continuous increase in the difference between the supply and demand of energy. Therefore, the future depends greatly on the discovery [11] of alternative energy sources and the enhanced efficiency of existing ones. Combined cycle power plants offer an efficient solution for electricity generation, making them a highly effective method to meet energy demands. Efficient operation relies on performance analysis to guarantee optimal functioning [14]. Several studies have been conducted on CCPP, and this section aims to review and summarize their findings. Cihan et al. [15] conducted a complete assessment of a natural gas-based CCPP, using working information from the units to conduct detailed exergy and energy analyses depending on the findings. The gas turbines (GTs), combustion chambers (CCs), and heat-recovery steam generators (HRSGs) were shown to be the primary cause of the irreversibilities, contributing to over 85% of the total exergy loss and exergy destruction. Reddy and Mohamed [16] analyzed how a natural gas-fired combined cycle power plant (CCPP) unit's energy destruction and efficiency are affected by its pressure ratio PR and intake GT temperature. Their findings unveiled the best pressure ratio at a constant inlet GT temperature, minimizing exergy destruction. Ameri et al. [17] evaluated the Neka natural gas-fired CCPP (420 MW) using exergy analysis, finding over 83% of irreversibility from HRSG, duct burner, combustion chamber, and gas turbine, with the greatest exergy loss coming from the combustion chamber. Gogoi et al. [18] presented a CCPP integrating a Rankine cycle (RC), Bryton cycle (BC), and recovering regenerative ORCs, achieving 54.22 MW with 44.79% energy efficiency and 40.89% exergy efficiency, with R123 as the optimal fluid. It cost USD 1965.43/h and showed significant exergy destruction in the combustion chamber and high capital costs for the gas turbine. Kalina [19] explored heat recovery configurations in combined gas turbine (GT) and steam turbine (ST) cycle power plants. They proposed modifying the hot side temperature profile and installing two gas turbines with a shared single-pressure heat recovery steam generator and two alternative heat exchanger designs to improve conventional systems. Kilani et al. [20] analyzed two CCPPs, focusing on steam-injection systems. Design 1 generates steam in the HRSG, while design 2 uses a heat-recovery system from the compressor outlet. Both have a Rankine cycle (RC) with two pressure abstraction levels. Steam injection improves efficiency, mainly when generated outside the HRSG. Aliyu et al. [21] analyzed a triple-pressure CCPP with reheat facilities, focusing on temperature gradients and exergy destruction. Critical parameters like the superheat pressure, reheat pressure, and steam quality significantly affected turbine output and efficiencies. Solar energy stands out in terms of various renewable energy sources as more desirable for delivering thermal electricity for power generation [22]. RES offers sustainability and can meet the world's energy demand. Hence, employing hybrid systems that combine fossil fuels with renewable energy (RE) can effectively mitigate fuel consumption while overcoming barriers associated with RES [23]. Enhancing plant efficiency and decreasing energy generation costs can be achieved by employing a hybrid power plant to meet energy demands. Numerous research studies focus on integrating the RES with the CCHP to enhance power plant efficiency and increase output power. For instance, Adibhatla et al. [24] conducted economic, exergy, and energy (3E) analyses on a power station integrated into a natural gas CCPP. Using direct steam generation (DSG) with parabolic trough collectors (PTCs), feed water preheated and evaporated in the solar field enhanced plant performance. The study showed energy and exergy efficiencies of 53.79% and 27.39%, respectively, with a 7.84% increase in plant output and a reduction in electricity generation costs from 7.4 to 6.7 cents/kWh. Akroot and Al Shammre [25] developed an SPRC system for electricity in Aden, Yemen, featuring PTCs, an RC, and a thermal

storage tank. A 4E investigation revealed that the system produces a 50 MW net with 30.7% exergetic and 32.4% energy efficiency. Nourpour et al. [26] investigated the ISCC in Yazd, Iran, using thermodynamic, exergy, exergoeconomic, and exergoenvironmental analyses based on Life Cycle Assessment (LCA). The ISCC achieved 48.25% thermal efficiency and 419,600 kW net power, with the equipment showing less than 10% avoidable exergy destruction, costs, and environmental impacts. Bonforte et al. [27] studied the integration of PTC solar power into CCPPs in Southern Poland to improve environmental performance. Their model predicted plant performance and exergy balance, showing that solar integration reduced CO_2 emissions by 9% and slightly increased capital costs, making it an attractive and cost-effective solution. Shoaei et al. [28] proposed a hybrid energy system with a BC, RC, two ORCs, and renewable sources using CPVT panels. Optimal ORC fluids were R123 and ammonia. The system achieved 50.59% energy efficiency and 25.44% exergy efficiency, generating 524.66 kW of power. Annual costs were USD 107,034, with monthly CO_2 emissions of 11,672 kg and 35,401 kg. Optimization improved exergy efficiency by 0.25% and reduced costs by USD 500 annually. Akroot et al. [29] studied hybrid energy systems for Libya's Sarir power plant. They proposed an ISCC system with a closed BC, an RC using PTCs with waste heat, and an organic Rankine cycle. Javadi et al. [30] examined the Iranian Abadan CCPP and proposed three configurations for a solar power tower SPT. The first, preheating inlet fuel, achieved 42.56% energy and 39.42% exergy efficiency, reducing emissions by 8041 tons/year. The second, preheating inlet air, reached 51.38% energy and 41.75% exergy efficiency, saving USD 11 million annually and cutting emissions by 34,563 tons/year. Using a dual-pressure heat-recovery steam generator, the third achieved 47.8% energy and 40.97% exergy efficiency, with the maximum power output at 370.4 MW. Talal et al. [31,32] recovered waste heat from BC in an Iraqi city called the Al-Qayara power station and integrated it with SPT. The plant's capacity is 561.5 MW, with 130.4 MW from waste heat and 68 MW from CSP.

This study introduces a new hybrid solar–natural gas-driven system, integrating a gas turbine unit (K1) and a solar parabolic trough collector (PTC), RC, and ORCs to create a poly-generation system for power production. An inclusive 4E analysis—encompassing energy, exergy, environmental, and exergoeconomic—has been conducted to thoroughly evaluate and understand the proposed system. The system is designed explicitly for the Kirkuk Power Plant in Iraq. A deep understanding of the features and limitations of Kirkuk, located in Northern Iraq with substantial solar radiation potential, is essential for justifying the implementation of this system. Utilizing solar energy alongside the waste heat from the Brayton cycle unit (K1) could significantly enhance the electricity output of the existing plant. The primary aim of this hybrid system is not only to boost power generation but also to reduce environmental pollution. Additionally, the results of this study will give insightful information and serve as a foundation for power plant engineers, operators, and designers.

2. System Description

Figure 1 illustrates the layout of the Kirkuk gas power plant in Iraq, which serves as the case study for this research. The plant comprises three units of gas turbines: K_1, K_2, and K_3. This study focuses on unit K_1, a Siemens V94.3A gas turbine model, which typically has an electrical output capacity of approximately 150 megawatts (MW).

Figure 2 displays the suggested hybrid system's outline involving the Brayton cycle (BC). It begins with the air compressor (AC) compressing air into the combustion chamber (CC), where it mixes with NG and burns. The resulting combustion gases drive the gas turbine (GT), producing energy in the generator (GEN). An integrated system combining RC and ORCs is added to maximize the benefit of the high-temperature exhaust gases discharged into the environment. Additionally, the system is enhanced with a PTC solar field to boost power output from the steam Rankine cycle by leveraging the substantial solar radiation potential in Kirkuk City. The working fluid selected for the ORCs is R123 due to its numerous advantages in combined power plant cycles, particularly in Organic

Rankine Cycles (ORCs). R123's low boiling point allows for the efficient recovery of low-temperature waste heat, significantly enhancing overall system efficiency [33]. Additionally, it boasts excellent thermal efficiency, making it ideal for lower-temperature heat sources such as geothermal energy or waste heat from primary cycles. R123 is also non-flammable, chemically stable, and provides a safer option for operational use.

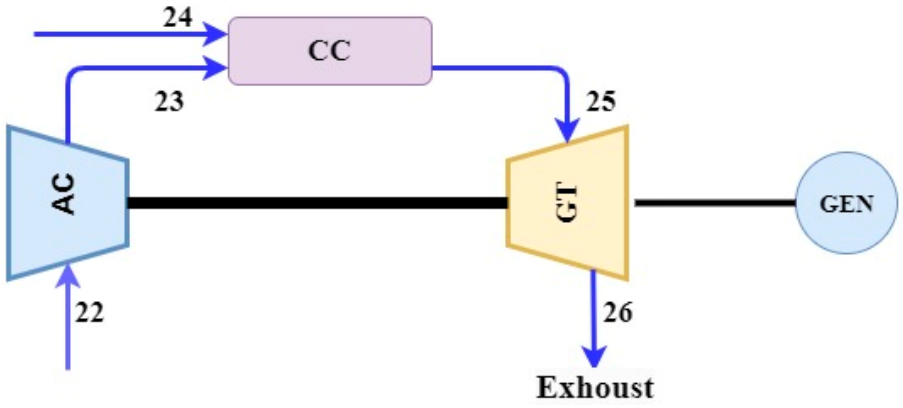

Figure 1. Gas turbine schematic diagram.

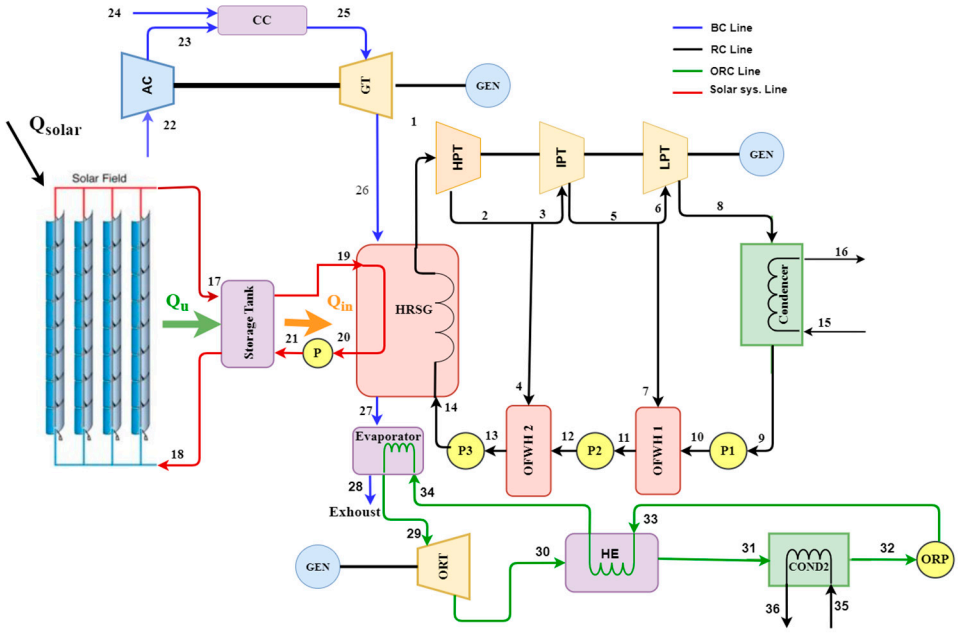

Figure 2. Diagram of the suggested hybrid system.

3. Methodology

3.1. Input Data and Assumption

The evaluation used Engineering Equation Solver (EES) software for analysis and modeling. The software calculates properties of thermodynamics, including temperature, exergy, pressure, and entropy. The fundamental parameters for entry of the proposed hybrid system are presented in Table 1. The assumptions used in the simulation are as follows:

- Negligible pressure drops, heat loss, and friction effects are assumed in heat exchangers and the pipe network.
- The difference between potential and kinetic energy is zero.
- The air compressor, pumps, and turbines are assumed to operate adiabatically.
- All processes within the cycle operate in an equilibrium state.
- Air is assumed to behave as an ideal gas.

- The sun's temperature is 5770 K [34].

Table 1. Input readings were utilized for the proposed hybrid system [35–37].

	Parameter	Value
GT cycle	Number of gas turbine unit	1
	GTIT, K	1376
	Mass flow rate of air, kg/s	438
	Compression ratio	9
	Ambient temperature, K	306
	LHV of fuel, (kJ/kg)	50,056
	RH	0.63
	η_{GT}, %	90
	η_{AC}, %	80
RC cycle	Inlet pressure for HPST, bar	100
	Inlet pressure for IPST, bar	40
	Inlet pressure for LPST, bar	10
	Condenser temperature, K	313
	η_{ST}, %	90
	η_{Pump}, %	85
ORCs	Inlet temperature for ORCs, K	471
	Inlet pressure for ORCs, bar	8
	Inlet pressure for ORCs, bar	1.2
	Working fluid	R123
	η_{ORT}, %	88
	η_{ORP}, %	80
TES system and solar field	Lat. (deg.)	35.47° N
	Long. (deg.)	44.39° E
	Position	Kirkuk/Iraq
	Solar field area (m^2)	510,120
	HTF's outlet temperature (°C)	565
	HTF's inlet temperature (°C)	287
	Working fluid	Salt (60% $NaNo_3$ −40% KNo_3)
	Area of collectors (m^2)	400,000
	DNI	8.02
	Reflection coefficient	0.94
	Receiver's absorption coefficient	0.92
	Transmission coefficient of the glass cover	0.92
	Incidence angle modifier	1
	η_{PTC}	85

3.2. System Analysis of Energy and Exergy

The system's mass, exergy, and energy equations are expressed individually for all components and the overall system. In a constant flow of the open system, the total mass inside the control volume remains constant over time. As per the principle of mass conservation, the total mass incoming to cv must be identical to the total mass exiting it. Moreover, in a constant flow open system, emphasis is placed on the mass flow rate ($\dot{m}$) per unit of time more than the total mass entering and leaving the system above a specific duration. Thus, the conservation of mass principle in generic constant flow systems with several inlets and outputs is represented as follows:

$$\sum \dot{m}_{in} = \sum \dot{m}_{out} \quad (1)$$

In constant-flow open systems, the control volume's overall energy content does not change (E_{cv} = constant). Consequently, the control volume's overall energy variation is zero (ΔE_{cv} = 0), indicating that the energy incoming to the cv equals the energy that exits it.

The energy conservation concept for an open system with continuous flow is expressed by the following equations [38,39]:

$$\sum \dot{E}_{in} = \sum \dot{E}_{out} \tag{2}$$

$$\dot{Q}_{in} + \dot{W}_{in} + \sum \dot{m}_{in} h_{in} = \dot{Q}_{out} + \dot{W}_{out} + \sum \dot{m}_{out} h_{out} \tag{3}$$

The following formula represents the energy-conservation principle for an open system with constant flow or the first law of thermodynamics. It takes into account the heat input that is brought into the system and used by the system to produce work [39–41]:

$$\dot{Q} + \dot{W} = \sum \dot{m}_{out} h_{out} - \sum \dot{m}_{in} h_{in} \tag{4}$$

The system's overall exergy balance can be expressed as follows [41,42]:

$$\sum \left(\dot{m}ex\right)_{in} + \dot{E}x_{in,W} + \dot{E}x_{in,Q} - \dot{E}x_{D} = \sum \left(\dot{m}ex\right)_{out} + \dot{E}x_{out,W} + \dot{E}x_{out,Q} \tag{5}$$

$$\dot{E}_{Q} = \dot{Q}\left(1 - \frac{T_0}{T_s}\right) \tag{6}$$

$$\dot{m}_{in}\, S_{in} + \left(\frac{\dot{Q}}{T}\right) + \dot{S}_{gen} = \dot{m}_{out}\, S_{out} \tag{7}$$

The parabolic solar collector's energy equations are shown below [42,43]. These formulas take into consideration two types of energy (thermal energy): input of solar energy $\dot{Q}_{Solar}$ derived from the total solar radiation and useful solar energy $\dot{Q}_u$ expressed as the heat transferred to the system. These energies are computed using the following equations:

$$\dot{Q}_{Solar} = A_A \cdot F_R \cdot S \cdot n_{cp}.n_{cs} \tag{8}$$

$$\dot{Q}_u = n_{cp} n_{cs} F_R [S A_a - A_r U_L (T_{ri} - T_o)] \tag{9}$$

In these equations, n_{cp}, n_{cs}, A_a, and A_r denote the collector's both parallel and series numbers, as well as the parabolic solar collector's aperture and receiving areas, respectively. F_R, S, and U_L symbolize the heat gain factor of the collector, the absorbed solar radiation amount, and the collector's heat loss coefficient, respectively. They are calculated using the following equations:

$$F_R = \frac{\dot{m}_c C_{p,c}}{A_r U_L}\left[1 - \exp\left(-\frac{U_L F' A_r}{\dot{m}_c C_{p,c}}\right)\right] \tag{10}$$

$$S = DNI \cdot \eta_{PTC} \cdot \gamma \cdot \tau \cdot \alpha \cdot K \tag{11}$$

$$F' = \frac{1/U_L}{\frac{1}{U_L} + \frac{D_{o,r}}{h_f D_{i,r}} + \left(\frac{D_{o,r}}{2k} \ln \frac{D_{0,r}}{D_{i,r}}\right)} \tag{12}$$

$$U_L = \left(\frac{A_R}{(h_w + h_{rc}) \cdot A_G} + \frac{1}{h_{rr}}\right)^{-1} \tag{13}$$

$$\dot{E}_{Q_{solar}} = \dot{Q}_{solar}\left(1 - \frac{T_0}{T_{Sun}}\right) \tag{14}$$

The collector modeling incorporates various parameters such as γ (reflection coefficient), τ (transmission coefficient of the glass cover), α (receiver's absorption coefficient), and K (incidence angle modifier). These parameters are detailed in Table 2, which provides the input data for the collector.

Table 2. Exergy and energy balance equations for each component of the proposed hybrid system.

Elements	Energy Equation's Balance	Exergy Equation's Balances
Compressor	$\dot{W}_{AC} = \dot{m}_{22}\,(h_{23} - h_{22})$	$\dot{E}_{D,AC} = \dot{W}_{AC} + \dot{E}_{22} - \dot{E}_{23}$
Combustion chamber	$\dot{m}_{23}h_{23} + \dot{m}_{24}LHV = \dot{m}_{25}h_{25}$	$\dot{E}_{D,CC} = \left(\dot{E}_{23} + \dot{E}_{24}\right) - \dot{E}_{25}$
Gas turbine	$\dot{W}_{GT} = \dot{m}_{25}(h_{25} - h_{26})$	$\dot{E}_{D,GT} = \left(\dot{E}_{25} - \dot{E}_{26}\right) - \dot{W}_{GT}$
HRSG	$\dot{Q}_{HRSG} = \dot{m}_{26}(h_{26} - h_{27}) + \dot{m}_{19}(h_{19} - h_{20}) = \dot{m}_{14}(h_1 - h_{14})$	$\dot{E}_{D,HRSG} = \dot{E}_{26} - \dot{E}_{27} + \dot{E}_{19} - \dot{E}_{20} - \dot{E}_{14} - \dot{E}_1$
HPST	$\dot{W}_{HPST} = \dot{m}_1(h_1 - h_2)$	$\dot{E}_{D,HPST} = \dot{E}_1 - \dot{E}_2 - \dot{W}_{HPST}$
IPST	$\dot{W}_{IPST} = \dot{m}_3(h_3 - h_5)$	$\dot{E}_{D,IPST} = \dot{E}_3 - \dot{E}_5 - \dot{W}_{IPST}$
LPST	$\dot{W}_{LPST} = \dot{m}_6(h_6 - h_8)$	$\dot{E}_{D,LPST} = \dot{E}_6 - \dot{E}_8 - \dot{W}_{LPST}$
Condenser1	$\dot{Q}_{Con} = \dot{m}_{15}(h_{16} - h_{15})$	$\dot{E}_{D,Con} = \dot{E}_8 - \dot{E}_9 + \dot{E}_{15} - \dot{E}_{16}$
Condenser2	$\dot{Q}_{Con2} = \dot{m}_{34}(h_{35} - h_{34})$	$\dot{E}_{D,Con} = \dot{E}_{31} - \dot{E}_{32} + \dot{E}_{34} - \dot{E}_{35}$
Pump	$\dot{W}_{Pump} = \dot{m}_{20}(h_{21} - h_{20})$	$\dot{E}_{D,P} = \dot{W}_{P1} + \dot{E}_{20} - \dot{E}_{21}$
Pump1	$\dot{W}_{Pump1} = \dot{m}_9(h_{10} - h_9)$	$\dot{E}_{D,P1} = \dot{W}_{P1} + \dot{E}_9 - \dot{E}_{10}$
Pump2	$\dot{W}_{Pump2} = \dot{m}_{11}(h_{12} - h_{11})$	$\dot{E}_{D,P2} = \dot{W}_{P2} + \dot{E}_{11} - \dot{E}_{12}$
Pump3	$\dot{W}_{Pump3} = \dot{m}_{13}(h_{14} - h_{13})$	$\dot{E}_{D,P3} = \dot{W}_{P1} + \dot{E}_{13} - \dot{E}_{14}$
OFWH1	$\dot{Q}_{OFWH1} = \dot{m}_{10}h_{10} + \dot{m}_7h_7 = \dot{m}_{11}h_{11}$	$\dot{E}_{D,OFWH1} = \dot{E}_7 + \dot{E}_{10} - \dot{E}_{11}$
OFWH2	$\dot{Q}_{OFWH2} = \dot{m}_{12}h_{12} + \dot{m}_4h_4 = \dot{m}_{13}h_{13}$	$\dot{E}_{D,OFWH2} = \dot{E}_4 + \dot{E}_{12} - \dot{E}_{13}$
ORT	$\dot{W}_{ORT} = \dot{m}_{29}(h_{29} - h_{30})$	$\dot{E}_{D,ST} = \dot{E}_{29} + \dot{E}_{30} - \dot{W}_{ORT}$
Heat exchanger	$\dot{Q}_{HE} = \dot{m}_{30}(h_{30} - h_{31})$	$\dot{E}_{D,HE} = \dot{E}_{30} + \dot{E}_{33} - \dot{E}_{31} - \dot{E}_{34}$
ORP	$\dot{W}_{ORP} = \dot{m}_{33}(h_{33} - h_{32})$	$\dot{E}_{D,ORP} = \dot{W}_{ORP} + \dot{E}_{32} - \dot{E}_{33}$
Evap	$\dot{Q}_{Evap} = \dot{m}_{27}(h_{27} - h_{28}) = \dot{m}_{29}(h_{29} - h_{34})$	$\dot{E}_{D,Evap} = \dot{E}_{27} - \dot{E}_{28} + \dot{E}_{34} - \dot{E}_{29}$
Solar	$\dot{Q}_{solar} = \eta_{PTC} * A_{ap} * DNI = \dot{m}_{17}(h_{17} - h_{18})$	$\dot{E}_{Q,solar} = \left(1 - \frac{T_0}{T_{sun}}\right)\dot{Q}_{solar}$
TES	$\dot{Q}_{TST} = \dot{m}_{17}(h_{17} - h_{18}) = \dot{m}_{19}\,(h_{19} - h_{21})$	$\dot{E}_{DTST} = \dot{E}_{17} + \dot{E}_{21} - \dot{E}_{19} - \dot{E}_{18}$

Though solar radiation energy entering the system is computed using the above-mentioned formulas, The following formula can be used to calculate the total solar collecting area [42]:

$$A_a = \dot{Q}_{solar}(w - D_{a,r})L \tag{15}$$

The exergy destruction Ex_{dest} of all components will be quantified utilizing the exergy equilibrium calculation [44].

$$\dot{E}_q - \dot{E}_w = \sum \dot{E}_{out} - \sum \dot{E}_{in} - \dot{E}_D \tag{16}$$

The exergy destruction Ex_{dest} rate, heat loss H_{Loss} exergy rate, and power exergy are represented, respectively, as $\dot{E}_D$, $\dot{E}_q$, and $\dot{E}_w$. Calculating $\dot{E}_Q$ and $\dot{E}_w$ is determined as follows:

$$\dot{E}_Q = \left(1 - \frac{T_0}{T_i}\right)\dot{Q}_i \tag{17}$$

$$\dot{E}_w = \dot{W}_i \tag{18}$$

The indicated hybrid system's components exergy and energy balance equations are shown in Table 2.

The energy performance denoted as η_{th} can be estimated using the following equation:

$$\eta_{th} = \frac{\dot{W}_{GT} - \dot{W}_{AC} + \dot{W}_{HPST} + \dot{W}_{IPST} + \dot{W}_{LPST} - \dot{W}_{Pumps} + \dot{W}_{ORT} - \dot{W}_{ORP}}{\dot{Q}_{in} + \dot{Q}_{solar}} \quad (19)$$

The amount of heat supplied to the cycle was estimated from

$$\dot{Q}_{in} = \dot{m}_{fuel} LHV\, \eta_{CC} \quad (20)$$

Moreover, the exergy efficiency (η_{ex}) serves as an indicator of system's quality and is calculable by means of the following formula:

$$\eta_{ex} = \frac{\dot{W}_{GT} - \dot{W}_{AC} + \dot{W}_{HPST} + \dot{W}_{IPST} + \dot{W}_{LPST} - \dot{W}_{Pumps} + \dot{W}_{ORT} - \dot{W}_{ORP}}{\dot{E}_3 + \dot{E}_{Q_{solar}}} \quad (21)$$

where E is the exergy of the fuel that was supplied to the cycle combustion chamber.

3.3. Exergoeconomic and Environmental Analysis

The examination of exergoeconomics includes determining the cost balance per each system component. The fundamental equation for determining the cost balance of the following is a representation of each system component in thermoeconomics [45,46]:

$$\sum_e \dot{C}_{e,k} + \dot{C}_{w,k} = +\sum_i \dot{C}_{i,k} + \dot{Z}_k \quad (22)$$

$$\dot{C}_j = c_j \dot{E}_j \quad (23)$$

Here, $\dot{C}$ denotes the rate of cost (USD/h), and $\dot{Z}_k$ represents the overall rate of the cost associated with capital investment and maintenance costs and operation for component k. The following equation is used to obtain the overall investment cost rate:

$$\dot{Z}_k = \frac{Z_k \cdot CRF \cdot \varphi}{N \times 3600} \quad (24)$$

The maintenance factor, represented by φ in this context, is fixed at 1.06. N is the total number of hours the system runs in a year, or 8000 h [47]. A number representing the rate of return on invested capital is called the Capital Recovery Factor (CRF). The equations detailing the balance cost for all components in the hybrid system are presented in Table 2. These equations are presented together with the related auxiliary equations and underlying assumptions:

$$CRF = \frac{(i(1+i)^n)}{((1+i)^n - 1)} \quad (25)$$

It is assumed that the interest rate, indicated by the letter "i", and a life span system, expressed by the letter "n", are 10% and 20 years, respectively [42]. Moreover, exergoeconomic analysis studies the system via particular performance indicators. These contain the Ex_{dest} cost rate, the cost per unit exergy of fuel and product, and the exergoeconomic factor, which is explained as follows [48]:

$$c_{F,k} = \dot{C}_{F,k} / \dot{E}_{F,k} \quad (26)$$

For each component k in the fuel stream, $c_{P,k}$ is the expense rate per unit exergy flow. The component cost rate for the fuel supply is indicated by the letter $c_{F,k}$. The exergy flow rate of the fuel stream's components is expressed by $\dot{E}_{P,k}$ stream [49]:

$$c_{P,k} = \dot{C}_{P,k} / \dot{E}_{P,k} \quad (27)$$

where $c_{p,k}$ is the cost rate (CR) per unit exergy flow for all components in the product stream, $\dot{C}_{p,k}$ denotes the CR associated with components in the product stream, and $\dot{E}_{p,k}$ represents the exergy flow rate of the component in the product stream. The cost rate related to the e Ex_{dest} of all components is determined as follows [50]:

$$\dot{C}_{D,k} = c_{F,k}\dot{E}_{D,k} \tag{28}$$

where $\dot{C}_{D,K}$ represents the cost rate related to the Ex_{dest} of the component. $\dot{E}_{D,K}$ represents the Ex_{dest} rate of the component. Table 3 presents the cost balance and auxiliary equations for the system components. The exergoeconomic factor for the component is calculated as follows [51]:

$$f_k = \dot{Z}_k / \left(\dot{Z}_k + c_{F,k}\dot{E}_{D,k} + \dot{E}_{L,k}\right) \tag{29}$$

Table 3. Cost balance and auxiliary equations of the system components [52,53].

Component	Cost Balance Equation	Auxiliary Equation
AC	$\dot{C}_{22} + \dot{C}_{W,AC} + \dot{Z}_{AC} = \dot{C}_{23}$	$c_{w,AC} = c_{w,GT}$
CC	$\dot{C}_{23} + \dot{C}_{24} + \dot{Z}_{CC} = \dot{C}_{25}$	$\frac{\dot{C}_{23}}{\dot{E}_{23}} = \frac{\dot{C}_{25}}{25}$, $c_{24} = 12$
GT	$\dot{C}_{25} + \dot{Z}_{W,GT} = \dot{C}_{26} + \dot{C}_{GT}$	$\frac{\dot{C}_{25}}{\dot{E}_{25}} = \frac{\dot{C}_{26}}{\dot{E}_{26}}$
HRSG	$\dot{C}_{26} + \dot{C}_{19} + \dot{C}_{14} + \dot{Z}_{HRSG} = \dot{C}_1 + \dot{C}_{27} + \dot{C}_{20}$	$\frac{26}{\dot{E}_{26}} = \frac{\dot{C}_{27}}{\dot{E}_{27}}$
HPST	$\dot{C}_1 + \dot{Z}_{W,HPST} = \dot{C}_2 + \dot{C}_{HPST}$	$\frac{\dot{C}_1}{\dot{E}_1} = \frac{\dot{C}_2}{\dot{E}_2}$
IPST	$\dot{C}_3 + \dot{Z}_{W,IPST} = \dot{C}_5 + \dot{C}_{IPST}$	$\frac{\dot{C}_3}{\dot{E}_3} = \frac{\dot{C}_5}{\dot{E}_5}$
LPST	$\dot{C}_6 + \dot{Z}_{W,LPST} = \dot{C}_8 + \dot{C}_{LPST}$	$\frac{\dot{C}_6}{\dot{E}_6} = \frac{\dot{C}_8}{\dot{E}_8}$
Cond1	$\dot{C}_8 + \dot{C}_{15} + \dot{Z}_{cond1} = \dot{C}_9 + \dot{C}_{16}$	$\frac{\dot{C}_8}{\dot{E}_8} = \frac{\dot{C}_9}{\dot{E}_9}$
Pump1	$\dot{C}_9 + \dot{C}_{W,P1} + \dot{Z}_{P1} = \dot{C}_{10}$	$c_{w,P1} = c_{w,HPST}$
OFWH1	$\dot{C}_7 + \dot{C}_{10} + \dot{Z}_{OFWH1} = \dot{C}_{11}$	
Pump2	$\dot{C}_{11} + \dot{C}_{W,P2} + \dot{Z}_{P2} = \dot{C}_{12}$	$c_{w,P2} = c_{w,HPST}$
OFWH2	$\dot{C}_{12} + \dot{C}_4 + \dot{Z}_{OFWH2} = \dot{C}_{13}$	
Pump3	$\dot{C}_{13} + \dot{C}_{W,P3} + \dot{Z}_{P3} = \dot{C}_{14}$	$c_{w,P3} = c_{w,HPST}$
PTC	$\dot{C}_{18} + \dot{C}_{q,solar} + \dot{Z}_{PTC} = \dot{C}_{17}$	$\dot{C}_{q,solar} = 0$
TES	$\dot{C}_{17} + \dot{C}_{21} + \dot{Z}_{TES} = \dot{C}_{18} + \dot{C}_{19}$	
Pump4	$\dot{C}_{20} + \dot{C}_{W,P4} + \dot{Z}_{P4} = \dot{C}_{21}$	$c_{w,P4} = c_{w,HPST}$
Evap	$\dot{C}_{27} + \dot{C}_{34} + \dot{Z}_{Evap} = \dot{C}_{28} + \dot{C}_{29}$	$\frac{\dot{C}_{27}}{\dot{E}_{27}} = \frac{\dot{C}_{28}}{\dot{E}_{28}}$
ORT	$\dot{C}_{29} + \dot{Z}_{W,ORT} = \dot{C}_{30} + \dot{C}_{ORT}$	$\frac{\dot{C}_{29}}{\dot{E}_{29}} = \frac{\dot{C}_{30}}{\dot{E}_{30}}$
HE	$\dot{C}_{30} + \dot{C}_{33} + \dot{Z}_{HE} = \dot{C}_{31} + \dot{C}_{34}$	$\frac{\dot{C}_{30}}{\dot{E}_{30}} = \frac{\dot{C}_{31}}{\dot{E}_{31}}$
Cond2	$\dot{C}_{31} + \dot{C}_{35} + \dot{Z}_{cond2} = \dot{C}_{32} + \dot{C}_{36}$	$\frac{\dot{C}_{31}}{\dot{E}_{31}} = \frac{\dot{C}_{32}}{\dot{E}_{32}}$
ORP	$\dot{C}_{32} + \dot{C}_{W,ORP} + \dot{Z}_{ORP} = \dot{C}_{33}$	$c_{w,ORP} = c_{w,ORP}$

Finally, the CO_2 emission rate (ϵ_{CO_2}) is calculated using the following equation [54]:

$$\epsilon_{CO_2} = \frac{\dot{m}_{CO_2}}{\dot{W}_{net}} \quad (30)$$

4. Discussion and Results

Three steps are involved in the thermodynamics and exergoeconomic analysis of the present coupled system. Initially, the developed model is validated through comparisons with findings from previous studies. The system operates under predefined conditions in the second stage, serving as the baseline scenario. Finally, parametric experiments are conducted in the third stage to explore how the system performs under different operational scenarios.

4.1. Validation

Table 4 compares the numerical findings obtained from prior simulation research [55] and the current investigation conducted on a gas turbine unit located in Kirkuk. The differences between the literature and the current investigations are minimal, suggesting that the present study's findings are consistent and dependable compared to the prior simulation study. The exhaust temperature exhibits the most notable variance, with a magnitude of 2.1%, whilst the other measurements show negligible disparities. The literature study reports a fuel flow rate of 8.8 kg/s, while the present study shows a slightly higher rate of 8.84 kg/s, resulting in a deviation of 0.45%. The outlet compressor temperature in the literature study is 315.7 °C, compared to 318 °C in the present study, yielding a deviation of 0.723%. The maximum temperature in the literature study is 1100 °C, while the present study records 1111 °C, leading to a deviation of 1%. The exhaust temperature is 500 °C in the literature study and 510.6 °C in the present study, showing a deviation of 2.1%. The literature study indicates a power output of 150 MW, whereas the present study shows 148.7 MW, resulting in a deviation of 0.87%. Thermal efficiency is 34% in the literature study and 33.8% in the present study, with a deviation of 0.59%.

Table 4. Comparison of numerical results with a previous simulation study [55] on the Kirkuk gas turbine unit.

Parameter	Unit	Literature Study	Present Study	Deviation (%)
Ambient temperature	°C	19	19	0%
Pressure ratio (PR)	-	12	12	0%
Flow rate of air mass	kg/s	438	438	0%
Flow rate of fuel mass	kg/s	8.8	8.84	0.45%
Outlet compressor temperature	°C	315.7	318	0.723%
Maximum temperature	°C	1100	1111	1%
Exhaust temperature	°C	500	510.6	2.1%
Power output	MW	150	148.7	0.87
Thermal efficiency	%	34	33.8	0.59%

4.2. Base Case

Table 5 presents the electrical power produced and consumed by each component of the developed system. This information facilitates comparisons between the power-generation capacities of each cycle and the efficiencies resulting from integrating various processes into the bottoming cycle BC. Adding an organic and steam Rankine cycle to the base bottoming cycle yields an extra 123.25 MW of electricity generation compared to

the Brayton cycle alone. The table shows that the output of the work net $\dot{W}_{net}$ developed system reaches 240.8 MW, with η_{th} and η_{ex} efficiencies of 59.32% and 57.28%, respectively.

Table 5. Output quantities obtained using the integrated system model.

Output Quantity	Value
Power supplied for ACs, MW	142.6
Power output for GTs, MW	260.9
Power output for HPST, MW	28.333
Power output for IPST, MW	30.602
Power output for LPST, MW	60.624
Power supplied of P1, kW	103
Power supplied of P2, kW	358
Power supplied of P3, kW	843
Heat supplied to ORCs, MW	30.471
Power output for ORT, MW	5.01
Power supplied for ORP, kW	73.73
Required fuel (kg/s)	7.982
Work net by the system, MW	240.8
Overall energy efficiency, %	59.32
Overall exergy efficiency, %	57.28

Table 6 and Figure 3 display the fundamental exergy evaluation outcomes for the several developed system components. The findings present that higher exergy destruction typically correlates with lower exergy efficiency. Components with the highest energy transformations, like CC, HRSG, and PTCs, exhibit the most significant losses. These components achieve 45.49%, 21.8%, and 19.34% exergy destruction ratios, respectively. High-exergy-efficiency components like GT (95.76%), HPST (95.32%), IPST (93.8%), and LPST (90.52%) are essential for energy conversion system efficiency. These components transform energy into useful work with little losses. Finally, the proposed system reached a η_{Ex} of 58.39%.

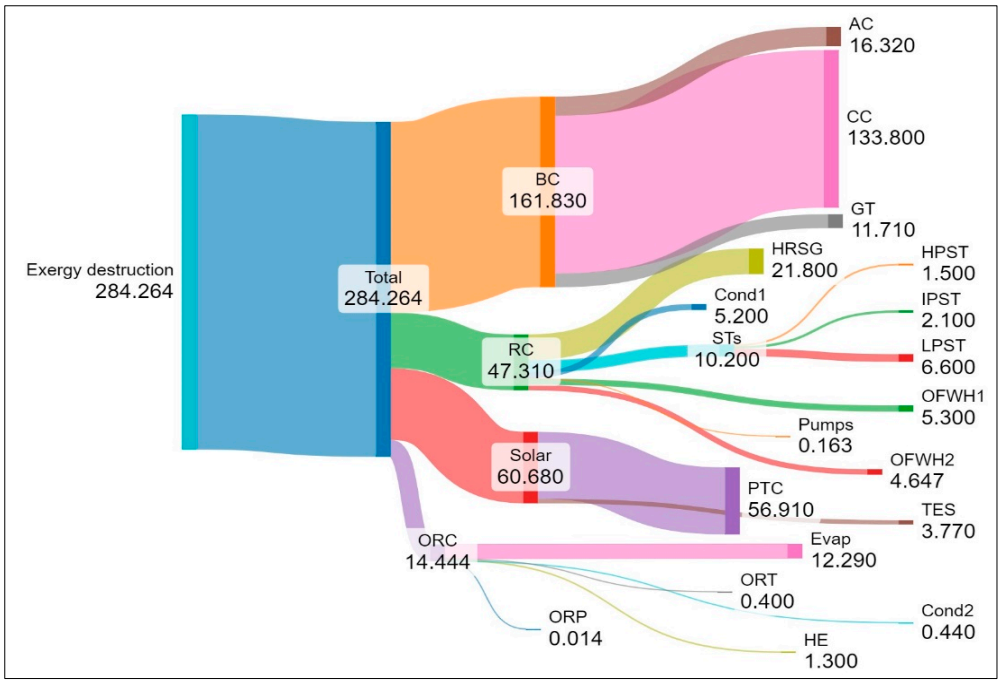

Figure 3. Ex_{dest} rates of the developed hybrid system parts.

Table 6. The integrated hybrid system model's energy evaluation findings.

Part	$\dot{E}_F$ (MW)	$\dot{E}_P$ (MW)	$\dot{E}_{destruction}$ (MW)	$\dot{E}_{destruction}$ (%)	Ψ (%)
AC	151.5	135.2	16.32	5.547	89.27
CC	555.5	421.7	133.8	45.49	75.91
GT	276.1	264.4	11.71	3.978	95.76
HRSG	175.7	153.9	21.8	7.407	78.59
HPST	30.9	29.46	1.448	0.492	95.32
IPST	33.92	31.82	2.103	0.7145	93.8
LPST	69.63	63.03	6.6	2.243	90.52
Cond1	10.67	5.471	5.202	1.768	51.26
Pump1	0.1071	0.09193	0.01513	0.001543	85.86
OFWH1	9.221	3.922	5.3	1.801	42.53
Pump 2	0.3722	0.3282	0.04397	0.01494	88.18
OFWH2	17.96	13.31	4.647	1.579	74.12
Pump 3	0.8769	0.7888	0.08803	0.02992	89.96
PTC	120.2	63.34	56.91	19.34	52.67
TST	63.34	59.57	3.766	1.28	94.05
EVAP	19.5	7.213	12.29	4.177	36.98
ORG T	5.407	5.013	0.3942	0.1339	92.71
HE	2.012	0.6793	1.333	0.4529	33.76
Cond2	0.5319	0.08809	0.4438	0.1508	16.56
Pump4	0.0738	0.05947	0.01432	0.004867	80.95

Table 7 shows the exergoeconomic results of components of the suggested hybrid system. Also, the flow chart presented in Figure 4 displays the total cost rate (USD/h), the cost of destruction (USD/h), and the Ex_{dest} rate (MW) of the proposed hybrid system and individual components. The central circle indicates the rate of the total cost for the system. Each arrow pointing away from the central circle represents an individual hybrid system component. The total Ex_{dest} rate for the proposed system is approximately 284.264 MW, with a total cost rate of around USD 17,041/h and an exergetic destruction cost of approximately USD 13,355/h. The PTCs exhibit the highest Ex_{dest} at nearly 56.91 MW and a total cost rate of USD 2210/h. The total cost of the suggested exergoeconomic hybrid system is USD 17,041.39/h, with an exergoeconomic factor of 20.8%.

Table 7. Exergo-economic results of parts of the integrated hybrid system model.

Component	c_f (USD/GJ)	c_p (USD/GJ)	$\dot{C}_D$ (USD/h)	$\dot{Z}_K$ (USD/h)	$\dot{C}=\dot{Z}_K+\dot{C}_D$ (USD/h)	f (%)
AC	21.02	22.3	852.6	247.4	1100	22.49
CC	14.61	19.4	7079	0.173	7079.2	0.002445
GT	19.4	20.53	832.1	234.4	1066.5	21.98
HRSG	16.17	18.62	1155	151.1	1306.1	11.57
HPST	20.32	22.51	101.8	122.15	223.95	54.53
IPST	20.32	22.83	147.9	128.92	276.82	46.57
LPST	20.32	23.4	464.3	208	672.3	30.94

Table 7. *Cont.*

Component	c_f (USD/GJ)	c_p (USD/GJ)	$\dot{C}_D$ (USD/h)	$\dot{Z}_K$ (USD/h)	$\dot{C}=\dot{Z}_K+\dot{C}_D$ (USD/h)	f (%)
Cond	20.32	39.79	366	2.98	368.98	0.8073
Pump1	23.4	31.9	1.226	1.48	2.706	54.69
OFWH1	20.43	53.86	374.9	78.624	453.52	17.33
Pump 2	23.4	29.68	3.563	3.59	7.153	50.15
OFWH2	27.81	39.41	447.6	87.372	535	16.33
Pump 3	23.4	28.42	7.132	6.584	13.716	48.01
PTC	0	125.6	0	2210	2210	100
TST	9.693	10.31	131.4	0.648	132	0.491
EVAP	19.4	52.89	857.8	11.02	868.82	10.45
ORT	65.15	73.55	92.37	59	151.37	39
HE	65.15	193	312.4	0.072	463.7	0.0231
Condenser2	65.15	404.3	104	3.452	107.45	3.215
Pump 4	6.43	7.198	1.96	0.14	2.1	6.626
Total			13,333.05	3557.11	17,041.39	20.8

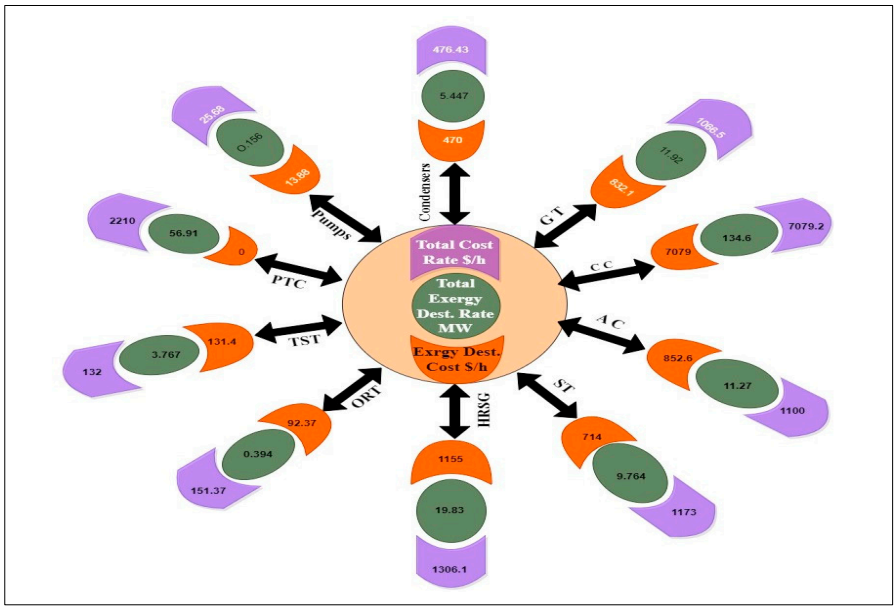

Figure 4. Flow chart of total cost rate, exergy cost, and Ex_{dest} rate of the proposed hybrid system.

4.3. Parametric Studies Results

Figure 5 illustrates the impact of the compressor pressure ratio PR on the developed performance of the system, cost, and carbon footprint. The findings show that the network output decreases while η_{th} and η_{ex} efficiencies increase with higher pressure ratios. This proposes a trade-off between efficiency gains and the amount of work that can be extracted. Higher pressure ratios demand more energy from the compressors, leading to decreased power generation from the bottoming cycle BC. Additionally, an increase in the PR negatively affects the Rankine cycle's RC power output. This occurs because a higher PR reduces the gas turbine's exhaust temperature, diminishing the energy available for the RC cycle. Consequently, the RC's mass flow rate decreases, reducing power generation. According to Figure 4, increasing the PR from 6 to 15 reduces the system's total $\dot{W}_{net}$ output

from 245.3 MW to 201.1 MW. The analysis reveals that an increase in the BC pressure ratio leads to a concomitant decrease in both the total $\dot{W}_{net}$ and the fuel consumption of the cycle. The decline in fuel consumption is demonstrably more significant than the reduction in $\dot{W}_{net}$. It translates to lower energy and exergy inputs into the system, ultimately enhancing overall efficiencies for the combined cycle. As depicted in the figure, η_{th} rises with the PR, starting at 57.89% for a compressor pressure ratio of 6 and rising to 62.38% at a compressor pressure ratio of 15. Similarly, the exergy efficiency also improves with the pressure ratio, from 55.9% at a compressor pressure ratio of 6 to 60.23% at a PR of 15. The energy cost decreased as the PR increased, reaching a minimum point before rising at higher pressure ratios. The data indicated that the optimal pressure ratio was 8 bars, corresponding to the lowest energy cost of USD 71.93/MWh. This subsequent increase in cost is attributed to the higher expenses of BC component materials associated with a higher compressor pressure ratio. Furthermore, the decline in fuel consumption associated with an increased PR also reduces the CO_2 mass flow rate at the exhaust, leading to lower CO_2 emissions. Reducing the carbon footprint with higher pressure ratios is a significant positive outcome, indicating that optimizing pressure ratios can contribute to more sustainable energy production. The carbon footprint decreases as the pressure ratio increases, from 340.8 kg CO_2/MWh at a PR of 6 to 316.3 kg CO_2/MWh at a compressor PR of 15. This demonstrates that higher pressure ratios result in lower greenhouse gas emissions per unit of energy generated.

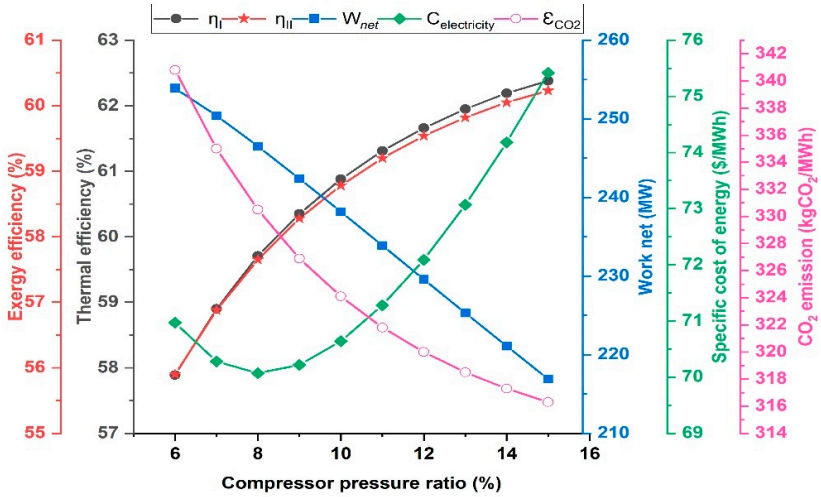

Figure 5. The effect of the compressor pressure ratio (PR) on the developed system's environment, performance, and cost.

Figure 6 demonstrates the impact of the gas turbine inlet temperature (GTIT) on the developed system's performance, environmental footprint, and energy costs. The parametric study of the GTIT presumes constant efficiencies for both the turbine and compressor. In actuality, alterations in the gas turbine's operating point impact both efficiencies, diminishing the total performance advantages. Increasing the GTIT increases power production across the bottoming BC, RC, and Organic Rankine Cycles (ORCs). The rise in GTIT leads to higher exhaust temperatures from the GT, thereby increasing the energy available for the RC and ORCs to utilize. Consequently, this results in a higher mass flow rate in the RC and ORCs, enhancing their power-production capabilities and improving the efficiency and power output of the entire cycle. Figure 6 shows that the $\dot{W}_{net}$ output substantially increases with the GTIT, rising from 150.6 MW at 1100 K to 339.7 MW at 1600 K. As the GTIT increases, the overall efficiencies of the developed system improve rather than decrease. This improvement results from a concurrent increase in the cycle's overall $\dot{W}_{net}$ and fuel consumption, which occurs at higher GTIT levels. The increased fuel consumption leads to more energy and exergy inputs into the system, which are compensated by the enhanced total power output, thus raising the system's overall

efficiencies. The results show that thermal efficiency experiences minor variations as the GTIT increases. It starts at 59.99% when the temperature is 1100 K and peaks at 60.65% when it reaches 1450 K. Beyond this, it stabilizes at around 60.5% as the temperature rises to 1600 K. The exergy efficiency remains relatively stable throughout the temperature range, fluctuating slightly between 57.93% at 1100 K and 58.47% at 1600 K. The findings illustrate that higher GTITs enhance thermal efficiency and significantly boost work output, which can lead to lower costs up to a specific temperature—in this case, 1400 K. Beyond this temperature, the costs increase slightly. The figure shows that energy costs initially drop from 97.76 USD/MWh at 1100 K to USD 70.29/MWh at 1400 K, then stabilize and rise again, reaching 81.02 USD/MWh at 1600 K. The lowest cost corresponds to the peak in thermal efficiency. The optimal range for cost efficiency is identified between 1400 K and 1450 K, where energy costs are minimized and thermal efficiency is maximized. Furthermore, although the CO_2 mass flow rate at the exhaust increases with higher GTIT values, the carbon footprint remains relatively stable, showing minimal variation despite changes in GTIT. This stability is credited to the increased total power output facilitated by the higher GTIT, compensating for the rise in the CO_2 mass flow rate. As a result, the carbon footprint stays relatively constant, around 326 kg CO_2/MWh, across most temperature settings, with only a slight increase to 329.5 kg CO_2/MWh as the temperature reaches 1600 K.

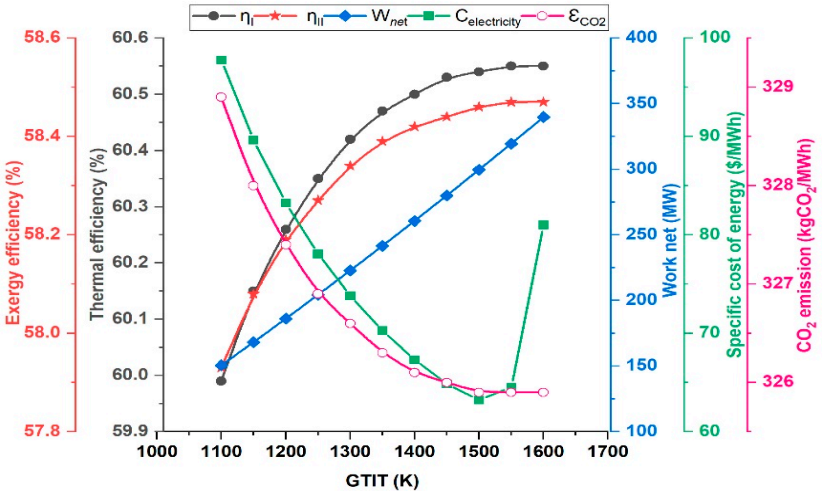

Figure 6. The influence of the temperature of the GTIT on the developed system's performance, environment, and cost.

Figure 7 evaluates how the input temperature T_1 of the HPST affects the developed system's performance, environmental effect, and cost indicators. While the bottoming cycle's power output remains constant, the Rankine cycle's power output decreases as T_1 is reduced. This decline is attributed to the lower T_1, which minimizes the enthalpy of the working fluid at the HPST inlet, resulting in less energy available for the RC cycle to utilize and consequently leading to a decrease in both the $\dot{W}_{net}$ and efficiencies of the developed system. The net power output exhibits a downward trend with a reduction in temperature, falling from 241.6 MW at 813 K to 235.5 MW at 723 K. This trend is in line with the decreases in both η_{th} and η_{Ex} efficiencies, suggesting reduced energy conversion into work as temperatures decline. η_{th} generally decreases, starting at 60.47% and dropping to 58.95%, and η_{Ex} decreases from 58.39% at 813 K to 56.92% at 723 K. The findings also depicted that increasing the HPST inlet temperature has a positive impact on the system's economic performance and environmental impact. Reduced temperatures lead to lower efficiency and somewhat increased energy expenses, emphasizing the need to sustain higher temperatures for economically efficient operation. As the temperature falls, there is a slight rise in energy costs. The cost per (MWh) rises from 70.29 USD/MWh at a temperature of 813 K to 72.59 USD/MWh at a temperature of 723 K. The correlation between lower temperatures

and an increased carbon footprint highlights the negative environmental impact of diminished efficiency. This suggests that higher operating temperatures not only improve performance but also help to minimize carbon emissions. As the input temperature of the HPST rises, the mass flow rate of CO_2 at the exhaust remains constant. However, there is a slight reduction in CO_2 emissions for the whole system, which is connected to the rise in the overall $\dot{W}_{net}$ of the cycle as T_1 increases. The carbon footprint rises when the HPST intake temperature falls, going from 326.3 kg CO_2/MWh at 813 K to 334.7 kg CO_2/MWh at 723 K.

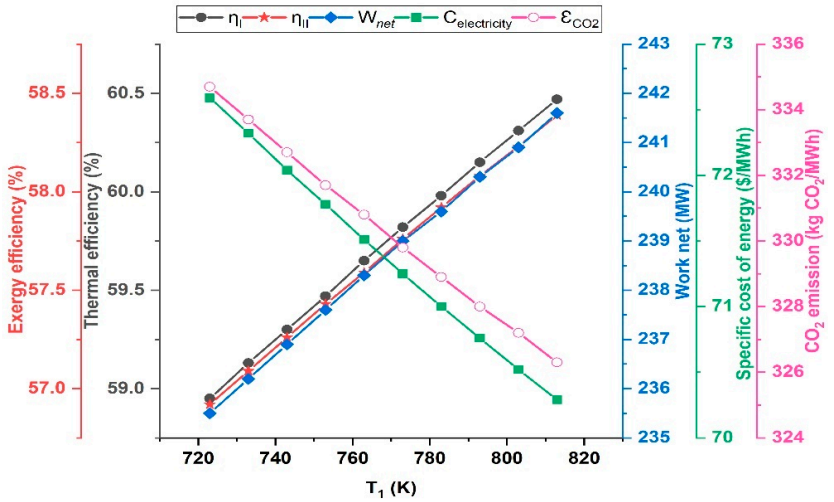

Figure 7. The influence of the HPST inlet temperature T_1 on the developed system's performance, environment, and cost.

The effect of changing the HPST inlet pressure P_1 on using the developed system, environmental impact, and cost are shown in Figure 8. The power output of the RC is directly proportional to both the mass flow rate of steam and the reduction in enthalpy across the turbine. Increasing the inlet pressures of the HPST, particularly when combined with elevated temperatures, increases the steam's specific enthalpy. This enhancement facilitates a more effective energy conversion during the expansion phase. Consequently, this typically caused increased power output and enhanced overall efficiencies of the developed system. The results indicate that the network output progressively increases with pressure, starting at 234.6 MW at 60 bar and peaking at 246.2 MW at 150 bar. Thermal efficiency rises from 58.71% to 61.63% as P_1 increases, while exergy efficiency increases from 56.7% at 60 bar to 59.51% at 150 bar. These results demonstrate that more significant pressures improve the system's energy conversion efficiency, suggesting that it converts energy into usable work more efficiently. The findings also show that raising the HPST inlet pressure enhances the performance of the system's economic and environmental effects. The results show that the HPST inlet pressure boosts efficiency and lowers energy costs. Rising pressure P lowers the energy cost from 74.56 USD /MWh to 67.6 USD /MWh at 150 bar. Increasing the HPST intake pressure reduces the carbon footprint, demonstrating the environmental benefits of better efficiency. These changes increase performance and decrease CO_2 emissions per unit of energy from 336 kg CO_2/MWh at 60 bar to 320.1 kg CO_2/MWh at 150 bar.

Figure 9 shows the effect of the condenser temperature T_8 on the developed system's performance, environmental effects, and cost indicators. Lowering the temperature of the condenser in a vapor power plant improves both power generation and overall system efficiency. Reduced temperatures result in a drop in turbine back pressure, enabling steam to expand farther. Consequently, this improves the means of changing heat energy into mechanical energy. Furthermore, the condensation process decreases entropy generation due to the increased heat release and higher density of steam. As a result, the exhaust temperature of the steam that exits the turbine is lower, which increases the variation in

temperature between the heat input in the boiler and the heat output in the condenser, thus increasing thermodynamic efficiency. The findings indicate that the power output exhibits an overall drop with increasing condenser temperature, implying that the system's capacity to work diminishes at higher condenser temperatures. The output power declines from 241.6 MW at 40 °C to 224.1 MW at 80 °C. As the condenser temperature rises, both the thermal and exergy efficiency decline. The thermal efficiency decreases from 60.47% at 40 °C to 56.1% at 80 °C. The exergy efficiency consistently follows a pattern of decline, decreasing from 58.39% to 54.17% over the given temperature range. The decrease in efficiency indicates that the system's capacity to transform heat into productive work decreases with higher condenser temperatures. The results also suggest that raising the condenser temperature has a contrary effect on both energy expenditure and carbon emissions. The rise in energy cost from 70.29 USD/MWh to 81.6 USD/MWh and carbon footprint from 326.3 kg CO_2/MWh to 351.7 kg CO_2/MWh reveals a direct economic effect from decreasing efficiency.

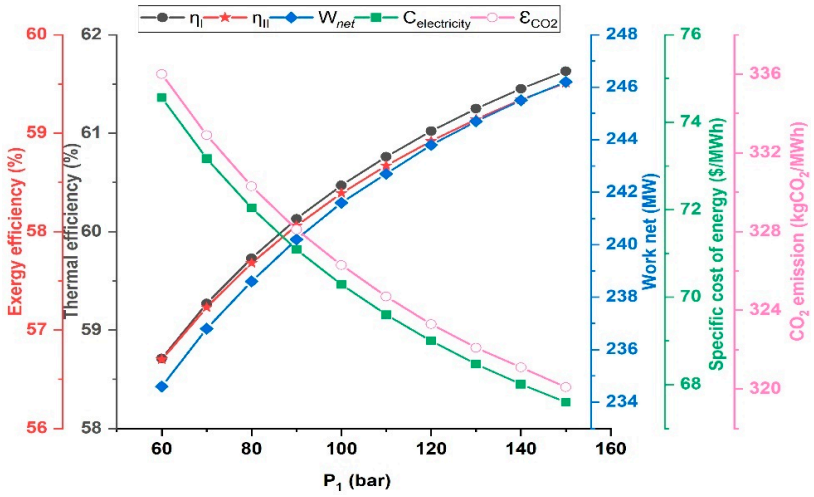

Figure 8. HPST inlet pressure P_1's effects on system performance, environment, and cost.

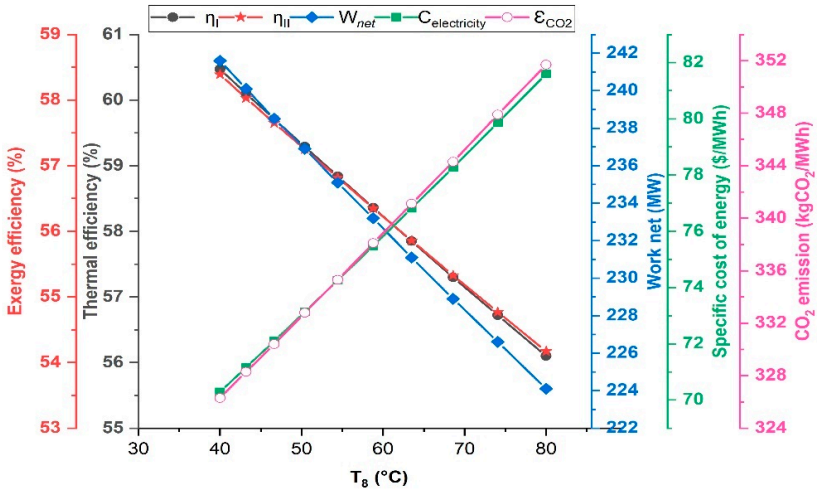

Figure 9. The impact of the condenser temperature on the developed system's performance, environment, and cost.

5. Conclusions

This research aims to examine and evaluate a newly developed hybrid system that merges a Kirkuk Brayton Cycle (BC) with both a steam Rankine cycle (RC) and an Organic Rankine Cycle (ORC). The energy for the proposed hybrid system is generated through natural gas and solar parabolic trough collectors (PTCs). The novel design combines the

benefits of fossil fuels and renewable energy, overcoming their respective limitations to achieve improved economic and environmental efficiency. The power plant in Kirkuk, a city in the northern region of Iraq, benefits significantly from the substantial solar radiation potential. As a result, it is an ideal location for the installation of this hybrid system. The current facility experiences a significant increase in power generation when solar energy is integrated with natural gas, and the excess heat from the gas turbine is efficiently utilized. The environmental effect assessment is an inclusive study that inspects CO_2 emissions and carbon footprint levels. It focuses on the system's capability to decrease greenhouse gas emissions effectively.

According to the findings, it can be determined that the hybrid system suggested in this study can augment electricity generation while also remaining environmentally economical and environmentally friendly. The conclusions offer valued recommendations that can suggestively increase the efficiency and functionality of hybrid power manufacturing systems, particularly in regions with ecological conditions comparable to Kirkuk's. The results of this study propose that integrating solar PTC systems with natural gas might present a capable method that supports the efficiency improvement and environmental sustainability of power production, contributing to the overall development of ecological energy solutions.

The results demonstrate notable improvements in both energy and exergy efficiency. With a thermal efficiency η_{th} of 59.32% and an η_{Ex} of 57.28%, the proposed system shows significant advancements over conventional power-generation methods. The exergoeconomic analysis offers valuable insights, revealing the lowest energy cost of 71.93 USD/MWh /MWh when the compressor pressure ratio is optimized at 8 bar. This underscores the importance of optimizing this parameter to minimize costs. Additionally, the environmental study indicates that increasing the compressor pressure ratio significantly reduces CO_2 emissions, lowering the carbon footprint to 316.3 kg CO_2/MWh. Overall, the hybrid system enhances electricity production while operating efficiently, cost-effectively, and sustainably. This study found that increasing the compressor pressure ratio improved both thermal and exergy efficiencies, with an optimal energy cost achieved at 8 bar. Raising the gas turbine inlet temperature (GTIT) from 1100 K to 1600 K significantly boosted the net power output, peaking at 339.7 MW, while maintaining stable CO_2 emissions. Similarly, increasing the HPST inlet pressure from 60 bar to 150 bar enhanced the thermal efficiency to 61.63% and exergy efficiency to 59.51% while also reducing energy costs and emissions. Higher HPST inlet temperatures, particularly at 813 K, further improved system performance by lowering energy costs and minimizing the carbon footprint.

Author Contributions: Conceptualization, A.A. (Abdulrazzak Akroot); Methodology, E.D.; Software, A.A. (Ali Alfaris) and A.A. (Abdulrazzak Akroot); Validation, A.A. (Abdulrazzak Akroot); Formal analysis, A.A. (Ali Alfaris); Investigation, A.A. (Ali Alfaris), A.A. (Abdulrazzak Akroot), and E.D.; Writing—original draft, A.A. (Ali Alfaris), A.A. (Abdulrazzak Akroot), and E.D.; Writing—review and editing, A.A. (Abdulrazzak Akroot). All authors have read and agreed to the published version of the manuscript.

Funding: This research received no external funding.

Institutional Review Board Statement: Not applicable.

Informed Consent Statement: Not applicable.

Data Availability Statement: The original contributions presented in the study are included in the article, further inquiries can be directed to the corresponding author.

Acknowledgments: All the authors are grateful to Karabuk University for providing its software and hardware infrastructure to realize the current study.

Conflicts of Interest: The authors declare no conflicts of interest.

Nomenclature

A*a*	Solar collector area (m^2)
$\dot{C}$	Cost rate, USD/h
DNI	Direct normal irradiation ($kWh/m^2 \cdot day$)
$\dot{E}x$	Exergy (kW)
$\dot{E}x_{dest}$	Rate of exergy destruction (kW)
f_k	Thermoeconomics factor (%)
F_R	Collector heat gain factor
h	Enthalpy (kJ/kg)
i	Interest rate
k	Conductivity heat transfer (W/m·K)
l	Insulation thickness (m)
$\dot{m}$	Mass flow rate (kg/s)
n	Predicted life of the system's (years)
$\dot{Q}$	Heat rate (kW)
$\dot{Q}_{solar}$	Solar energy input (kW)
s	Specific entropy (kJ/kg·K)
T	Temperature (K)
ν	Specific volume (m^3/kg)
$\dot{W}$	Work by the control volume per unit time (kW)
$\dot{Z}_k$	Entire cost rate
Greek Symbols	
η_{Ex}	Exergy efficiency (%)
η_{th}	Thermal efficiency (%)
α	Receiver's absorption coefficient
γ	Reflection coefficient
τ	Coefficient of the glass cover
φ	Total operating and maintenance cost
Abbreviations	
AC	Air compressor
BC	Brayton cycle
CC	Combustion chamber
CCPP	Combined cycle power plant
Cond	Condenser
CPVT	Concentrating photovoltaic thermal
CRF	Capital Recovery Factor
CSP	Concentrated solar power
cv	Control volume
DSG	Direct steam generation
EES	Engineering Equation Solver
EVAP	Evaporator
GHGs	Greenhouse gases
GT	Gas turbine
GTIT	Gas turbine inlet temperature
HE	Heat exchanger
HPST	High-pressure steam turbine
HRSG	Heat recovery steam generation
HTF	Heat transfer fluid
IPST	Intermediate-pressure steam turbine
ISCC	Integrated solar combined cycle
LCA	Life Cycle Assessment
LHV	Fuel's lower heating value
LPST	Low-pressure steam turbine
NG	Natural gas

NGCC	Natural gas combined cycle
OFWH	Open feed water heater
ORC	Organic Rankine Cycle
ORP	Organic pump
ORT	Organic turbine
PP	Power plant
PR	Pressure ratio
PTC	Parabolic trough collector
RC	Rankine cycle
RES	Renewable energy source
RH	Relative humidity
SPRC	Solar-powered Rankine cycle
SPT	Solar power tower
ST	Steam turbine
TES	Thermal energy storage
TST	Thermal storage tank
PEC	Purchase equipment cost

References

1. Espinosa-Cristia, J.F.; Breesam, Y.F.; Mrabet, B.M.; Nuñez Alvarez, J.R.; Abdullaev, S.S.; Kuzichkin, O.R.; Alhassan, M.S. Exergy and environmental analysis of a novel turbine inlet air cooling technique for power augmentation in a CCPP based on waste energy. *Chemosphere* **2023**, *338*, 139402. [CrossRef] [PubMed]
2. Thomas, C.D. Climate, climate change and range boundaries. *Divers. Distrib.* **2010**, *16*, 488–495. [CrossRef]
3. Yolcan, O.O. World energy outlook and state of renewable energy: 10-Year evaluation. *Innov. Green Dev.* **2023**, *2*, 100070. [CrossRef]
4. Cai, L.; Fu, Y.; Cheng, Z.; Xiang, Y.; Guan, Y. Advanced exergy and exergoeconomic analyses to evaluate the economy of LNG oxy-fuel combined cycle power plant. *J. Env. Chem. Eng.* **2022**, *10*, 108387. [CrossRef]
5. Kaushik, S.C.; Reddy, V.S.; Tyagi, S.K. Energy and exergy analyses of thermal power plants: A review. *Renew. Sustain. Energy Rev.* **2011**, *15*, 1857–1872. [CrossRef]
6. Saslow, W.M. A history of thermodynamics: The missing manual. *Entropy* **2020**, *22*, 77. [CrossRef] [PubMed]
7. Al-Hamadani, S. Solar energy as a potential contributor to help bridge the gap between electricity supply and growing demand in Iraq: A review. *Int. J. Adv. Appl. Sci.* **2020**, *9*, 302–312. [CrossRef]
8. Ibrahim, T.K.; Mohammed, M.K.; Awad, O.I.; Abdalla, A.N.; Basrawi, F.; Mohammed, M.N.; Najafi, G.; Mamat, R. A comprehensive review on the exergy analysis of combined cycle power plants. *Renew. Sustain. Energy Rev.* **2018**, *90*, 835–850. [CrossRef]
9. Shabgard, H.; Faghri, A. Exergy analysis in energy systems: Fundamentals and application. *Front. Heat. Mass. Transf.* **2019**, *12*. [CrossRef]
10. Zarza, E.; Valenzuela, L.; León, J.; Hennecke, K.; Eck, M.; Weyers, H.D.; Eickhoff, M. Direct steam generation in parabolic troughs: Final results and conclusions of the DISS project. *Energy* **2004**, *29*, 635–644. [CrossRef]
11. Jebasingh, V.K.; Herbert, G.M.J. A review of solar parabolic trough collector. *Renew. Sustain. Energy Rev.* **2016**, *54*, 1085–1091. [CrossRef]
12. Cabrera, F.J.; Fernández-García, A.; Silva, R.M.P.; Pérez-García, M. Use of parabolic trough solar collectors for solar refrigeration and air-conditioning applications. *Renew. Sustain. Energy Rev.* **2013**, *20*, 103–118. [CrossRef]
13. Eke, M.N.; Okoroigwe, E.C.; Umeh, S.I.; Okonkwo, P. Performance Improvement of a Gas Turbine Power Plant in Nigeria by Exergy Analysis: A Case of Geregu 1. *Open Access Libr. J.* **2020**, *7*, 1–20. [CrossRef]
14. Ersayin, E.; Ozgener, L. Performance analysis of combined cycle power plants: A case study. *Renew. Sustain. Energy Rev.* **2015**, *43*, 832–842. [CrossRef]
15. Cihan, A.; Hacihafizoğlu, O.; Kahveci, K. Energy-exergy analysis and modernization suggestions for a combined-cycle power plant. *Int. J. Energy Res.* **2006**, *30*, 115–126. [CrossRef]
16. Reddy, B.V.; Mohamed, K. Exergy analysis of a natural gas fired combined cycle power generation unit. *Int. J. Exergy* **2007**, *4*, 180–196. [CrossRef]
17. Ameri, M.; Ahmadi, P.; Khanmohammadi, S. Exergy analysis of a 420 MW combined cycle power plant. *Int. J. Energy Res.* **2008**, *32*, 175–183. [CrossRef]
18. Gogoi, T.K.; Lahon, D.; Nondy, J. Energy, exergy and exergoeconomic (3E) analyses of an organic Rankine cycle integrated combined cycle power plant. *Therm. Sci. Eng. Prog.* **2023**, *41*, 101849. [CrossRef]
19. Kalina, J. Analysis of alternative configurations of heat recovery process in small and medium scale combined cycle power plants. *Energy Convers. Manag.* **2017**, *152*, 13–21. [CrossRef]
20. Kilani, N.; Khir, T.; Ben Brahim, A. Performance analysis of two combined cycle power plants with different steam injection system design. *Int. J. Hydrog. Energy* **2017**, *42*, 12856–12864. [CrossRef]

21. Aliyu, M.; AlQudaihi, A.B.; Said, S.A.M.; Habib, M.A. Energy, exergy and parametric analysis of a combined cycle power plant. *Therm. Sci. Eng. Prog.* **2020**, *15*, 100450. [CrossRef]
22. Mehrpooya, M.; Ashouri, M.; Mohammadi, A. Thermoeconomic analysis and optimization of a regenerative two-stage organic Rankine cycle coupled with liquefied natural gas and solar energy. *Energy* **2017**, *126*, 899–914. [CrossRef]
23. Wang, S.; Zhang, G.; Fu, Z. Performance analysis of a novel integrated solar combined cycle with inlet air heating system. *Appl. Therm. Eng.* **2019**, *161*, 114010. [CrossRef]
24. Adibhatla, S.; Kaushik, S.C. Energy, exergy and economic (3E) analysis of integrated solar direct steam generation combined cycle power plant. *Sustain. Energy Technol. Assess.* **2017**, *20*, 88–97. [CrossRef]
25. Akroot, A.; Al Shammre, A.S. Techno-Economic and Environmental Impact Analysis of a 50 MW Solar-Powered Rankine Cycle System. *Processes* **2024**, *12*, 1059. [CrossRef]
26. Nourpour, M.; Khoshgoftar Manesh, M.H.; Pirozfar, A.; Delpisheh, M. Exergy, Exergoeconomic, Exergoenvironmental, Emergy-based Assessment and Advanced Exergy-based Analysis of an Integrated Solar Combined Cycle Power Plant. *Energy Environ.* **2023**, *34*, 379–406. [CrossRef]
27. Bonforte, G.; Buchgeister, J.; Manfrida, G.; Petela, K. Exergoeconomic and exergoenvironmental analysis of an integrated solar gas turbine/combined cycle power plant. *Energy* **2018**, *156*, 352–359. [CrossRef]
28. Shoaei, M.; Hajinezhad, A.; Moosavian, S.F. Design, energy, exergy, economy, and environment (4E) analysis, and multi-objective optimization of a novel integrated energy system based on solar and geothermal resources. *Energy* **2023**, *280*, 128162. [CrossRef]
29. Akroot, A.; Almaktar, M.; Alasali, F. The Integration of Renewable Energy into a Fossil Fuel Power Generation System in Oil-Producing Countries: A Case Study of an Integrated Solar Combined Cycle at the Sarir Power Plant. *Sustainability* **2024**, *16*, 4820. [CrossRef]
30. Javadi, M.A.; Jafari Najafi, N.; Khalili Abhari, M.; Jabery, R.; Pourtaba, H. 4E analysis of three different configurations of a combined cycle power plant integrated with a solar power tower system. *Sustain. Energy Technol. Assess.* **2021**, *48*, 101599. [CrossRef]
31. Talal, W.; Akroot, A. Exergoeconomic Analysis of an Integrated Solar Combined Cycle in the Al-Qayara Power Plant in Iraq. *Processes* **2023**, *11*, 656. [CrossRef]
32. Talal, W.; Akroot, A. An Exergoeconomic Evaluation of an Innovative Polygeneration System Using a Solar-Driven Rankine Cycle Integrated with the Al-Qayyara Gas Turbine Power Plant and the Absorption Refrigeration Cycle. *Machines* **2024**, *12*, 133. [CrossRef]
33. Li, M.; Wang, J.; He, W.; Gao, L.; Wang, B.; Ma, S.; Dai, Y. Construction and preliminary test of a low-temperature regenerative Organic Rankine Cycle (ORC) using R123. *Renew. Energy* **2013**, *57*, 216–222. [CrossRef]
34. Pavlovic, S.; Bellos, E.; Le Roux, W.G.; Stefanovic, V.; Tzivanidis, C. Experimental investigation and parametric analysis of a solar thermal dish collector with spiral absorber. *Appl. Therm. Eng.* **2017**, *121*, 126–135. [CrossRef]
35. Sachdeva, J.; Singh, O. Thermodynamic analysis of solar powered triple combined Brayton, Rankine and organic Rankine cycle for carbon free power. *Renew. Energy* **2019**, *139*, 765–780. [CrossRef]
36. Lugand, P.; Parietti, C. Combined cycle plants with frame 9F gas turbines. *Proc. ASME Turbo Expo.* **1990**, *4*, 475–481. [CrossRef]
37. Sabbaghi, M.A.; Soltani, M.; Rosen, M.A. A comprehensive 6E analysis of a novel multigeneration system powered by solar-biomass energies. *Energy* **2024**, *297*, 131209. [CrossRef]
38. Rodríguez, J.M.; Sánchez, D.; Martínez, G.S.; Bennouna, E.G.; Ikken, B. Techno-economic assessment of thermal energy storage solutions for a 1 MWe CSP-ORC power plant. *Sol. Energy* **2016**, *140*, 206–218. [CrossRef]
39. Chacartegui, R.; Vigna, L.; Becerra, J.A.; Verda, V. Analysis of two heat storage integrations for an Organic Rankine Cycle Parabolic trough solar power plant. *Energy Convers. Manag.* **2016**, *125*, 353–367. [CrossRef]
40. Sivakugan, N.; Shukla, S.K.; Das, B.M. *Fundamentals of Engineering Geology*; CRC Press: Boca Raton, FL, USA, 2020. [CrossRef]
41. Cengel, Y.A.; Boles, M.A. *Thermodynamics: An Engineering Approach*, 8th ed.; McGraw-Hill Education: New York, NY USA, 2015.
42. Aghaziarati, Z.; Aghdam, A.H. Thermoeconomic analysis of a novel combined cooling, heating and power system based on solar organic Rankine cycle and cascade refrigeration cycle. *Renew. Energy* **2021**, *164*, 1267–1283. [CrossRef]
43. Tehrani, S.S.M.; Taylor, R.A. Off-design simulation and performance of molten salt cavity receivers in solar tower plants under realistic operational modes and control strategies. *Appl. Energy* **2016**, *179*, 698–715. [CrossRef]
44. Ge, Y.; Wei, Y.; Zhao, Q.; Pei, Y. Energy and Exergy Analysis on a Waste Heat Recovery Module for Helicopters. *IEEE Access* **2021**, *9*, 122618–122625. [CrossRef]
45. Köse, Ö.; Koç, Y.; Yağlı, H. Energy, exergy, economy and environmental (4E) analysis and optimization of single, dual and triple configurations of the power systems: Rankine Cycle/Kalina Cycle, driven by a gas turbine. *Energy Convers. Manag.* **2021**, *227*, 113604. [CrossRef]
46. Akroot, A.; Al Shammre, A.S. Economic and Technical Assessing the Hybridization of Solar Combined Cycle System with Fossil Fuel and Rock Bed Thermal Energy Storage in Neom City. *Processes* **2024**, *12*, 1433. [CrossRef]
47. Mohammadkhani, F.; Shokati, N.; Mahmoudi, S.M.S.; Yari, M.; Rosen, M.A. Exergoeconomic assessment and parametric study of a Gas Turbine-Modular Helium Reactor combined with two Organic Rankine Cycles. *Energy* **2014**, *65*, 533–543. [CrossRef]
48. Assareh, E.; Hoseinzadeh, S.; Ghersi, D.E.; Farhadi, E.; Keykhah, S.; Lee, M. Energy, exergy, exergoeconomic, exergoenvironmental, and transient analysis of a gas-fired power plant-driven proposed system with combined Rankine cycle: Thermoelectric for power production under different weather conditions. *J. Therm. Anal. Calorim.* **2023**, *148*, 8283–8307. [CrossRef]

49. Besevli, B.; Kayabasi, E.; Akroot, A.; Talal, W.; Alfaris, A.; Assaf, Y.H.; Nawaf, M.Y.; Bdaiwi, M.; Khudhur, J. Technoeconomic Analysis of Oxygen-Supported Combined Systems for Recovering Waste Heat in an Iron-Steel Facility. *Appl. Sci.* **2024**, *14*, 2563. [CrossRef]
50. Alsunousi, M.; Kayabasi, E. Techno-economic assessment of a floating photovoltaic power plant assisted methanol production by hydrogenation of CO2 captured from Zawiya oil refinery. *Int. J. Hydrog. Energy* **2024**, *57*, 589–600. [CrossRef]
51. Kareem, A.F.; Akroot, A.; Abdul Wahhab, H.A.; Talal, W.; Ghazal, R.M.; Alfaris, A. Exergo–Economic and Parametric Analysis of Waste Heat Recovery from Taji Gas Turbines Power Plant Using Rankine Cycle and Organic Rankine Cycle. *Sustainability* **2023**, *15*, 9376. [CrossRef]
52. Zhang, F.; Yan, Y.; Liao, G.; Jiaqiang, E. Energy, exergy, exergoeconomic and exergoenvironmental analysis on a novel parallel double-effect absorption power cycle driven by the geothermal resource. *Energy Convers. Manag.* **2022**, *258*, 115473. [CrossRef]
53. Nazari, N.; Mousavi, S.; Mirjalili, S. Exergo-economic analysis and multi-objective multi-verse optimization of a solar/biomass-based trigeneration system using externally-fired gas turbine, organic Rankine cycle and absorption refrigeration cycle. *Appl. Therm. Eng.* **2021**, *191*, 116889. [CrossRef]
54. Tian, H.; Li, R.; Salah, B.; Thinh, P.H. Bi-objective optimization and environmental assessment of SOFC-based cogeneration system: Performance evaluation with various organic fluids. *Process Saf. Environ. Prot.* **2023**, *178*, 311–330. [CrossRef]
55. Ahmed, A.H.; Ahmed, A.M.; Hamid, Q.Y. Exergy and energy analysis of 150 MW gas turbine unit: A case study. *J. Adv. Res. Fluid. Mech. Therm. Sci.* **2020**, *67*, 186–192.